energies

MDPI

Article

Investigations on the Effect of Pre-Treatment of Wheat Straw on Ash-Related Issues in Chemical Looping Gasification (CLG) in Comparison with Woody Biomass

Florian Lebendig [1,*], Ibai Funcia [2], Rául Pérez-Vega [2] and Michael Müller [1]

[1] Forschungszentrum Jülich GmbH, Institute for Energy and Climate Research (IEK-2), Wilhelm-Johnen-Straße, 52428 Julich, Germany; mic.mueller@fz-juelich.de
[2] National Renewable Energy Centre, Av. Ciudad de la Innovación 7, 31621 Sarriguren, Spain; ifuncia@cener.com (I.F.); rperez@cener.com (R.P.-V.)
* Correspondence: f.lebendig@fz-juelich.de

Abstract: Biomass chemical looping gasification (BCLG) is a promising autothermic route for producing sustainable, N_2-free, and carbon neutral syngas for producing liquid biofuels or high value hydrocarbons. However, different ash-related issues, such as high-temperature corrosion, fouling and slagging, bed agglomeration, or poisoning of the oxygen carrier might cause significant ecologic and economic challenges for reliable implementation of BCLG. In this work, lab-scale investigations under gasification-like conditions at 950 °C and thermodynamic modelling were combined for assessing the influence of composition, pre-treatment methods, such as torrefaction and water-leaching, and Ca-based additives on the release and fate of volatile inorganics, as well as on ash melting behavior. A deep characterization of both (non-)condensable gas species and ash composition behavior, joint with thermodynamic modelling has shown that different pre-treatment methods and/or Ca-additives can significantly counteract the above-mentioned problems. It can be concluded that torrefaction alone is not suitable to obtain the desired effects in terms of ash melting behavior or release of problematic volatile species. However, very promising results were achieved when torrefied or water-leached wheat straw was blended with 2 wt% $CaCO_3$, since ash melting behavior was improved up to a similar level than woody biomass. Generally, both torrefaction and water-leaching reduced the amount of chlorine significantly.

Keywords: biomass; chemical looping gasification; pre-treatment; release and fate of inorganic species; agglomeration; fouling and slagging; high temperature corrosion; poisoning of oxygen carrier

Citation: Lebendig, F.; Funcia, I.; Pérez-Vega, R.; Müller, M. Investigations on the Effect of Pre-Treatment of Wheat Straw on Ash-Related Issues in Chemical Looping Gasification (CLG) in Comparison with Woody Biomass. *Energies* **2022**, *15*, 3422. https://doi.org/10.3390/en15093422

Academic Editors: Tomasz Czakiert and Jaroslaw Krzywanski

Received: 30 March 2022
Accepted: 4 May 2022
Published: 7 May 2022

1. Introduction

The Paris Agreement has proposed the reduction in carbon dioxide emissions throughout this century with the aim to limit the increase in the global average temperature to 2 °C or below [1]. In contrast to conventional fuels, which are based on fossil sources, biofuels are considered as CO_2-neutral alternatives for regenerative energy or syngas production. The fact that the produced CO_2 has previously been removed from the atmosphere via photosynthesis makes biomass-derived feedstocks promising candidates, since the emitted CO_2 can potentially be considered as neutral [2].

A very promising technology for producing sustainable synthetic fuels is chemical looping gasification (CLG), which represents an important part of the thermochemical Biomass-to-Liquid (BtL) route. The entire multistep process is described elsewhere [3]. Ishida et al. firstly proposed the term "chemical looping" [4]. The process generally describes the application of a metal oxide, which is used as an oxygen transport medium to perform a redox reaction scheme for an increase in energy efficiency in power generation. The CLG process is carried out at absence of nitrogen and therefore a syngas mixture of high purity can be achieved. Several advantages make CLG ecologically as well as economically

promising [5,6]. In addition to the lattice oxygen, the oxygen carrier provides heat for the endothermic gasification as well, which is beneficial due to the requirement of large energy supply for a stable operation. Moreover, the gas lower heating value is elevated because lattice oxygen derived from the oxygen carrier is more inclined to partially oxidize the biomass fuels in contrast to gas phase oxygen.

The CLG technology has been tested at laboratory scale up to 25 kW_{th} until now [7]. The CLG system is generally composed of two interconnected fluidized bed reactors, i.e., the fuel reactor, where the gasification of the fuel takes place, and the air reactor, where the oxygen carrier is re-oxidized after being reduced in the fuel reactor. A typical operation scheme of CLG demonstrating both fuel- and air-reactor is illustrated in Figure 1.

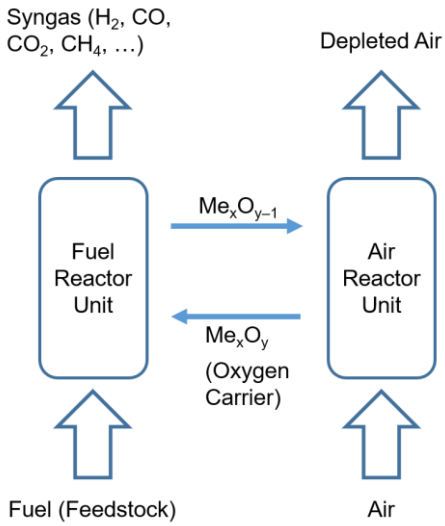

Figure 1. Schematic sketch of the chemical looping gasification process, modified after [8]. The reduced metal oxide Me_xO_{y-1} is circulated to the air reactor to be re-oxidized (Me_xO_y) before a new cycle starts.

The oxygen carrier "Me_xO_y" provides lattice oxygen for the gasification instead of molecular oxygen from the air. During the CLG process, several competing reactions occur, primarily divided into biomass pyrolysis and biomass gasification or ash/char reaction. The general process of biomass pyrolysis and subsequent char gasification or ash reaction can be described as follows [7]:

(i) Biomass pyrolysis:

$$C_nH_{2m}O_x \rightarrow \text{char} + \text{tar} + \text{syngas (CO, } H_2\text{, } CO_2\text{, } CH_4 \text{ and } C_nH_{2m}\text{)}, \quad (1)$$

(ii) Biomass gasification:

$$C + H_2O \rightarrow CO + H_2 \quad (2)$$

$$CH_4 + H_2O \rightarrow CO + 3\,H_2 \quad (3)$$

$$C + CO_2 \rightarrow 2\,CO_2 \quad (4)$$

The European research project CLARA (**C**hemical **L**ooping g**a**sification fo**r** Sustain**a**ble Production of Biofuels, Horizon 2020 framework program, G.A. 817841) [9], in which framework these investigations were performed, focuses on the use of biogenic residues, e.g., wheat straw, as CO_2 neutral fuel in CLG to produce liquid fuels via Fischer–Tropsch synthesis.

However, several ash-related challenges are expected to cause severe problems during CLG of biomass, as those fuels also cause problems in other conversion processes, which require sustainable solutions and have to be managed [10]. Since, for instance, herbaceous feedstocks have, in general, a higher ash content than woody feedstocks, it is necessary to

investigate and understand in detail the ash behavior and fundamental reaction mechanisms; most notably the ash-related issues. Herbaceous feedstocks, e.g., different straw varieties, have shown, among others, an extremely high chlorine content, which is directly related to chlorine-induced steel corrosion [11]. Moreover, the release as well as the transformation of certain problematic species, such as sulfur, potassium, silicon, or phosphorous lead to different ash-related operational problems during the conversion process. Alkalis, for instance, are known to form potassium or sodium silicates that have low melting points due to eutectic effects [12]. The amount of formed slag increases consequently, and bed agglomeration is significantly promoted. A further crucial aspect, which should be considered, is the phenomenon of fouling and slagging on the heat transfer surfaces, which is mainly caused by salts, generally alkali chlorides, but also carbonates or partly alkali sulfides. The presence of aggressive species in the feedstock's ash is well known to generate operational problems of heat exchanging surfaces in power boilers connected with fouling and slagging [13]. The ash-related operational problems listed above significantly reduce the total efficiency of gasifier systems, cause extra costs for cleaning and maintenance, and hinder utilization of biomass-derived fuels as gasifier fuels [14]. Concerning the formation and the transformation of problematic mineral phases during thermal processes (depending on the process parameters), many studies were conducted [15–17]. In addition to the ash content, different inorganic compounds (e.g., K, Na, Si, P, Ca, and Mg) in the ash are critical for determining ash-related problems [18–20].

Biomass pre-treatment is a necessary process step for thermochemical conversion of biomass, as it is required to improve its characteristics in order to enhance both efficiency of the biomass and the energy utilization [21,22]. Torrefaction is one method to produce biocoal, resulting in the removal of unbound water, improving heating values, better ignition, and combustion properties [23]. Moreover, torrefaction has shown the potential ability to significantly reduce the chlorine content of raw biomass [24]. Biomass leaching with water as a solvent is an effective method in order to remove problematic species, such as K/Na and Cl and to improve biomass feedstock properties for high temperature processes [25–27]. The nature of biomass ash has a strong impact on the ash melting behavior. The negative effect of low temperature ash melting can be overcome by adding calcium-based additives, which can better prevent sintering of biomass ash [28]. Most research is focused on analyzing fuel properties by leaching or (dry and wet) torrefaction [25,29–31], however, there are few studies on the combination of those methods plus using (Ca-based) additives.

The aim of this study was to investigate the influence of different pre-treatment methods, which are intended to mitigate ash-related issues, on the behavior of ash constituents of wheat straw. In particular, water-leaching, torrefaction, combination of both steps and/or blending feedstocks with additives (calcium carbonate in this work) were considered. Moreover, the interaction of different oxygen carrier materials with ash was investigated. To classify the effectiveness of the measures, industrial wood pellets were taken as benchmark material and pine forest residues were chosen as alternative woody waste biomass. Molecular Beam Mass Spectrometry (MBMS) was applied to investigate the release and the fate of inorganic volatile species during gasification. Ashes were characterized by X-ray diffraction (XRD) and ash fusion test. Lab-scale experiments were complemented by thermodynamic modelling using FactSage in order to predict release and condensation of volatile species, phase transformation in the ash, and potential reactions with oxygen carrier materials. Based on the obtained results, specific conclusions about the risk of bed agglomeration, slagging and fouling, high-temperature corrosion, and poisoning of oxygen carriers is discussed.

2. Materials and Methods

2.1. Materials, Pre-Treatment, and Chemical Characterisation

Wheat straw (harvested in Navarra, North of Spain) was selected as herbaceous feedstock in this study, because of its availability and potential use in Europe or worldwide in general. All feedstock samples were chemically and gravimetrically (ash content) characterized according to the European reference standards' specifics for solid biofuels (Table 1). Different pre-treatment methods were applied: Wheat straw was water-leached and/or torrefied, and additionally the samples were added with 2 wt% $CaCO_3$. Moreover, industrial wood pellets were taken as benchmark material and pine forest residues were selected as alternative woody waste biomass.

Table 1. Feedstock characterization according to the European reference standards.

Analysis	European Reference Standard
Ash content	UNE-EN-ISO18122
Ultimate analysis (C, H, and N)	UNE-EN-ISO 16948
Sulfur and Chlorine content	UNE-EN-ISO 16994
Major elements (ash components)	UNE-EN-ISO 16967

Instead of standard ashing at 550 °C with subsequent chemical analysis of major ash elements, direct microwave acid digestion of the fuels was applied prior to the determination by optical emission spectroscopy combined with inductively coupled plasma source (ICP/OES). This option was preferred in order to avoid the volatilization of substances caused by a pre-treatment in a muffle furnace. The ash content was determined gravimetrically at 550 °C. Each fuel sample was milled and sieved to a diameter of 0.56 mm to improve analytical investigations in further steps.

Samples were abbreviated as follows: To = torrefied sample, To-WL = first torrefied, then water-leached sample, To + A = sample including 2 wt% $CaCO_3$ as additive, To-WL + A = torrefied/water-leached sample including 2 wt% $CaCO_3$ as additive, IWP = industrial wood pellets and PFR = pine forest residues. The torrefaction procedure was realized inside of a torrefaction laboratory rotating batch reactor, which has been designed and constructed by CENER (Centro Nacional de Energías Renovables, Sarriguren, Spain), under the framework of the CLARA project. The reactor is electrically heated by an independent furnace, which can reach temperatures up to 300 °C. The temperature is controlled by three thermocouples located along the reactor. The torrefaction was carried out at 260 °C in an inert N_2-atmosphere (continuous fed of 360 L h^{-1}) for 30–40 min to avoid combustion of the sample material. The water-leaching process was carried out with deionized Milli-Q water for 24 h at room temperature (20 °C), and with a solid to liquid ration of 1:10 (solid about 100 g). In the last step, the solid was recovered by filtration and rinsed three times with 100 mL of deionized Milli-Q water. The wet samples were dried overnight at 45 °C until the moisture content became stable.

2.2. Thermodynamic Modelling

Thermodynamic equilibrium calculations, which are based on the minimization of Gibbs free energy, were realized to predict inorganic phase formation of ash constituents under gasification-like conditions, using the computational package FactSage™ 7.3 [32]. The commercial database SGPS was used for pure gaseous and some solid stoichiometric compounds. Additionally, the database GTOX, which has been developed in cooperation by Forschungszentrum Jülich and GTT-Technologies was used for the present work [33]. The chemical compositions of the corresponding fuel ashes were taken into consideration for thermodynamic equilibrium calculations. Phase formations under pyrolysis-like conditions were calculated without addition of steam and oxygen, while the phase formations under gasification-like conditions were calculated considering water (steam/feedstock = 0.5 g/g) and oxygen (Fe_2O_3/feedstock = 0.48 g/g, only the oxygen of the oxygen carrier Fe_2O_3 was

taken into account). It shall be noted that the latter assumes a full reduction in a completely oxidized oxygen carrier, which is likely not the case in the real process. However, the effectively supplied amount of oxygen is similar, so that a reasonable syngas composition was achieved.

A thermodynamic model comprising a sequence of several equilibrium reactors was designed to describe important steps of the CLG process, focusing on ash related issues. It shall be noted that only the gasification part of the process is represented by the model, whereas the air reactor for re-oxidation of the oxygen carrier materials is not considered. The scheme of the designed model is presented in Figure 2.

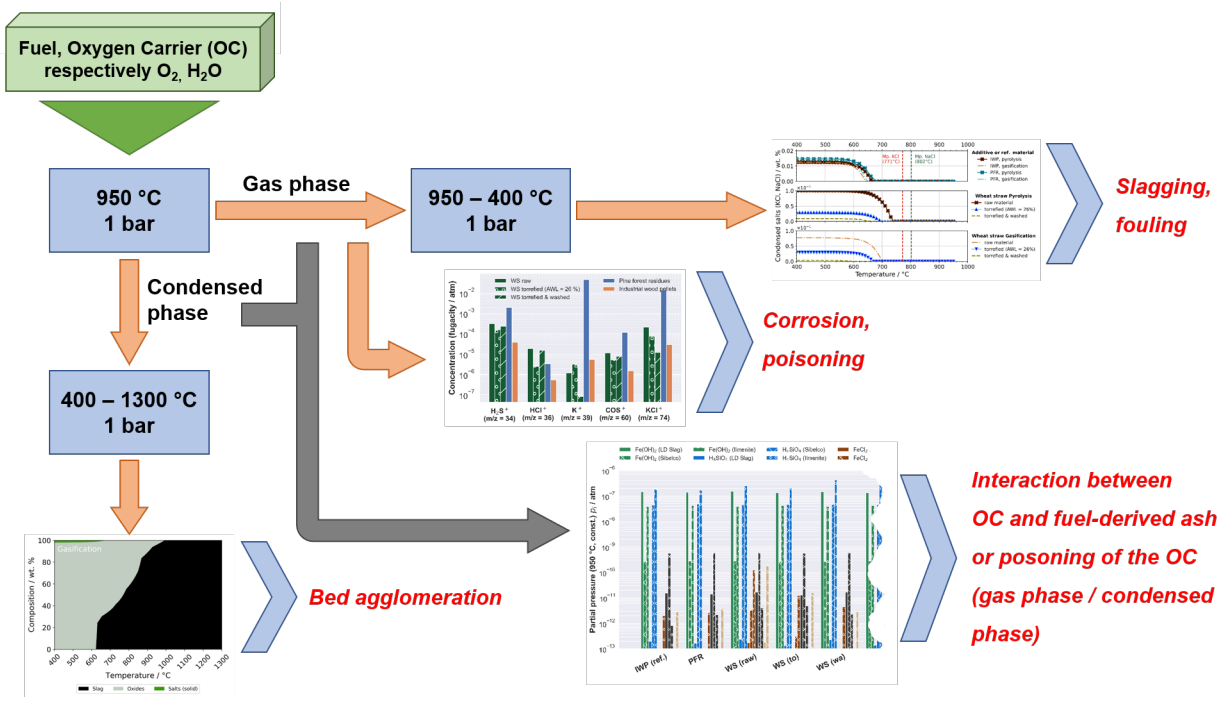

Figure 2. Scheme of the thermodynamic model for investigation of ash related issues in CLG. Equilibrium calculations were carried out with FactSage 7.3.

2.3. Experimental Hot Gas Analysis by Molecular Beam Mass Spectrometry (MBMS)

For the real-time determination of inorganic gaseous species released during gasification, a Molecular Beam Mass Spectrometer (MBMS) was used. The apparatus allows studies of hot gases from diverse origins in biomass-derived feedstocks under a gasification-like atmosphere. The general technique of a MBMS is based on common mass spectrometry, which analyzes the mass–to–charge ratios (m/z) in an electromagnetic field. A detailed description of the experimental setup of the MBMS can be found elsewhere [34,35].

Release experiments under gasification-like conditions at 950 °C were performed. A four-zone furnace was used and the alumina-tube inside the furnace was connected to the MBMS nozzle, which represents the gas inlet of the apparatus. Gasification of the sample took place within the first two zones at 950 °C. A temperature zone was set at 1400 °C to crack all formed hydrocarbons, as only inorganic species should be investigated. The setup of the tube furnace can be seen in other publications [34,35].

In total, three measurements were realized for each sample and averaged for semi-quantitative analyses and error calculations. The same atmospheric conditions as for the ashing procedure were used for the release experiments, i.e., 15 vol% H_2O-steam and 5 vol% CO_2 in He (to increase resolution of the MBMS). The total gas flow was set to 4 L/min for each experiment. Then, 50 mg of fuel was gasified in a single run. The samples were kept in the furnace for varying retention times, depending on the first overview of all spectra, from 2 min to max. 6 min and were characterized afterwards. The retention time reflects the reaction sequence, as species show different release behavior or, more precisely, only

devolatilization or subsequent char gasification and ash reaction. Intensity-time profiles of $^{23}CO_2{}^{++}$, $^{34}H_2S^+$, $^{35}Cl^+$, $^{36}HCl^+$, $^{37}Cl^+$, $^{38}HCl^+$, $^{39}K^+$, $^{47}PO^+$, $^{55}KO^+$, $^{58}NaCl^+$, $^{60}COS^+$, $^{62}P_2{}^+$, $^{63}PO_2{}^+$, $^{64}SO_2{}^+$, $^{74}KCl^+$, $^{81}Na_2Cl^+$, $^{97}NaKCl^+$, $^{106}P_2O_4{}^+$, $^{113}K_2Cl^+$, and $^{122}P_2O_5{}^+$ were recorded and normalized to the $^{23}CO_2{}^{++}$ base level signal for quantification.

2.4. Ash Sample Preparation for Ash Fusion Tests and X-ray Powder Diffractometric Analysis

Ash of each feedstock sample was produced under gasification-like conditions at constant temperature (550 °C). The gasifying medium comprised 15 vol% H_2O-steam in Ar, and 5 vol% CO_2 was added as substitution for the oxygen carrier. At the beginning of the process, a small amount of oxygen was added to accelerate the carbon conversion. A lambda sensor was used during the ashing procedure for controlling the partial pressure of oxygen. When the partial pressure of oxygen increased, the ashing procedure was almost completed and the oxygen supply was stopped to prevent oxidizing conditions or combustion. Afterwards, the ash samples were annealed at 550 °C for 3 h in an argon-hydrogen (Ar/4% H_2) atmosphere to ensure formation of crystalline compounds. The detection of crystalline compounds is indispensable for X-ray diffractometric investigation. For the determination of ash melting behavior by hot stage microscopy, the ash was pressed into a cylindrical pellet with a diameter of 5 mm (strength ~1.5 kN). One drop of pure isopropanol was added as surfactant to keep the pellet stable during the pressing process. Due to various carbon content (which affects the density of the sample material), the sample height varied between 4 mm to 7 mm. Note that the same amount of ash was weighed for each sample preparation.

2.5. Ash Fusion Test by Hot Stage Microscopy (HSM)

Hot stage microscopy was used for the determination of the melting behavior of the fuel ashes. The typical sample geometry is represented by a cylindrical pellet (Section 2.4), which is placed inside of a tube furnace. The furnace chamber was flushed with a constant flow of 13 vol% carbon dioxide and 87 vol% Argon. Based on equilibrium calculations, the defined amount of carbon dioxide was required to keep possibly formed carbonates stable. The furnace was heated from room temperature up to 1300 °C at 5 K/min. A CCD camera was placed behind the furnace outlet, and photos were taken at every degree Celsius. A corresponding software evaluated the change of the sample shape (height ratio of the pellet) in dependence of the temperature change. Depending on this information, conclusions can be drawn about the ash melting behavior. The evaluation is based on the ratio of current sample height/original sample height (coefficient h_x/h_0) according to Pang et al. [36].

3. Results

3.1. Experimnetal Part

3.1.1. Fuel Composition

Table 2 gives the proximate and ultimate analysis of the treated fuels. The torrefied samples have higher carbon contents, as compared to the raw wheat straw sample. Depending on the elements, the difference in the ash forming matter varies. The torrefied sample shows a higher concentration of Ca and K in contrast to the raw material, whereas the torrefied and subsequently water-leached sample shows a lower concentration of K, which might be explained by element-specific differences in the water solubility.

The bar diagram illustrates the difference of the ash content between herbaceous, as well as woody biomass (IWP/PFR), resulting from different amount of inorganics. Among other things, it can be observed that $CaCO_3$-additivation of the wheat straw samples increases the ash content evidently.

Table 2. Chemical composition of the pre-treated wheat straw samples as well as the benchmark materials. The actual contents in each fuel sample are presented on a dry solid basis. O was calculated by difference. To: torrefied, To-WL: torrefied/water-leached, To + A: torrefied plus 2 wt% $CaCO_3$, To-WL + A: torrefied/water-leached plus 2 wt% $CaCO_3$, IWP: industrial wood pellets and PFR: pine forest residues.

wt%	Raw	To	To-WL	To + A	To-WL + A	IWP	PFR
C	48.8	56.4	56	54.5	57.5	50.8	52.7
H	6.2	5.9	6.1	6.1	6.0	6.0	6.4
N	0.4	0.45	0.3	0.3	0.32	0.07	0.339
O	44.6	37.3	37.4	39.1	36.2	43.2	40.5
S	0.05	0.065	0.035	0.03	0.03	0.008	0.05
Ash components (major elements only)/mg kg^{-1}							
Cl	230	145	50	50	200	60	70
Al	846	1090	943	1540	1220	62	174
Ca	4060	5550	5140	11,700	13,700	1300	3390
Fe	860	7890	672	1430	1690	82	134
K	4720	5995	2070	7190	3970	486	1370
Mg	460	1001	775	944	909	232	453
Na	129	116	75	328	418	13	34
P	313	417	223	441	383	94	217
Si	7205	9455	7725	10,500	14,000	1050	958

Figure 3 shows the ash content of the pre-treated straw samples as well as PFR/IWP.

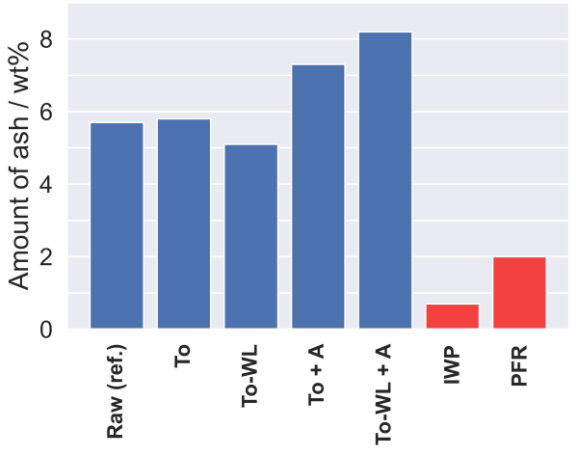

Figure 3. Amount of ash in dependence of different pre-treatment methods. The red bars denote the benchmark (IWP) as well as the alternative woody waste biomass (PFR). The ash contents are presented on a dry solid basis.

3.1.2. Experimental Hot Gas Analysis

Samples listed in Table 2 have been investigated by MBMS method regarding the release and fate of inorganic species. Both, devolatilization and char gasification/ash reaction were examined. To understand the influence of different pre-treatment methods and the release behavior of the most important species, a semi-quantitative analysis was performed, which allows the determination of relative peak intensities. The obtained results can be compared with each other semi quantitatively by means of bar diagrams; however, an absolute conclusion about the species content (e.g., absolute concentration of one species, such as KCl, SO_2, and so forth) cannot be drawn.

As an example, results of the MBMS-measurements for untreated wheat straw are shown in Figure 4. The depicted graph shows the intensity-time profiles of different inorganic species as a function of the measurement runtime. Although specific species showed a corresponding release behavior (e.g., $^{39}K^+$), other species showed only background noise

(e.g., $^{47}PO^{+}$). Conversely, the background noise means that no reaction in form of any release was observed.

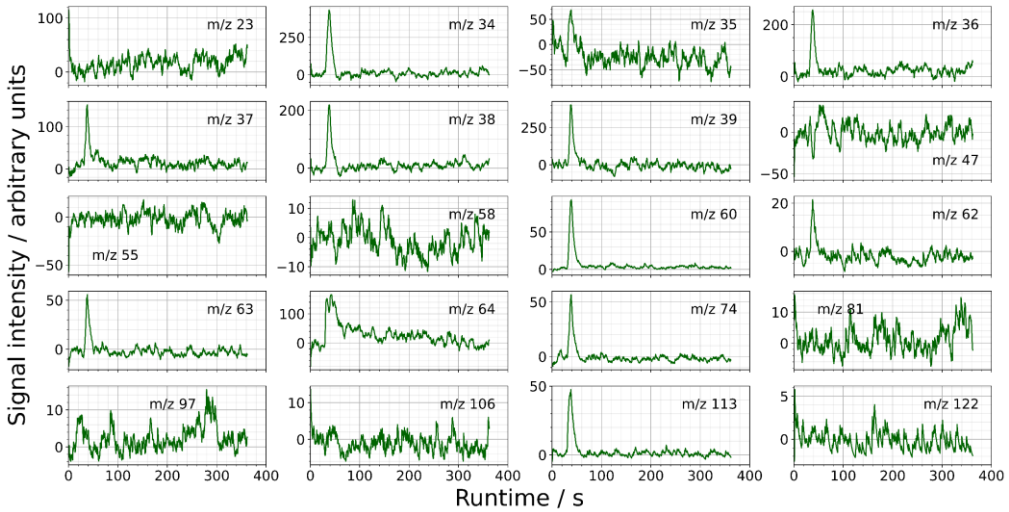

Figure 4. Intensity-time profiles of $^{23}CO_2^{++}$, $^{34}H_2S^{+}$, $^{35}Cl^{+}$, $^{36}HCl^{+}$, $^{37}Cl^{+}$, $^{38}HCl^{+}$, $^{39}K^{+}$, $^{47}PO^{+}$, $^{55}KO^{+}$, $^{58}NaCl^{+}$, $^{60}COS^{+}$, $^{62}P_2^{+}$, $^{63}PO_2^{+}$, $^{64}SO_2^{+}$, $^{74}KCl^{+}$, $^{81}Na_2Cl^{+}$, $^{97}NaKCl^{+}$, $^{106}P_2O_4^{+}$, $^{113}K_2Cl^{+}$, and $^{122}P_2O_5^{+}$ gained for raw wheat straw at 950 °C in 80 vol% He, 15 vol% H_2O and 5 vol% CO_2.

Recorded mass spectra of sulfur dioxide are presented in Figure 5.

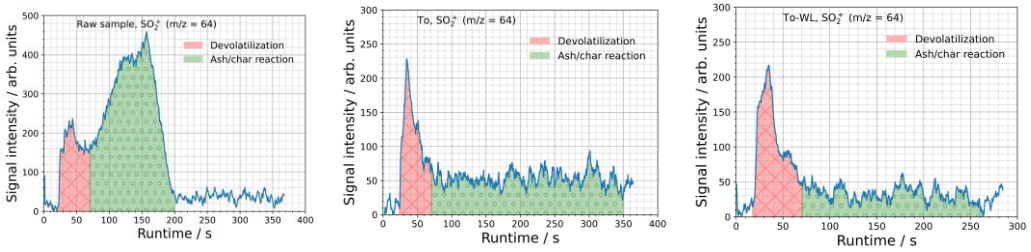

(**a**) (**b**) (**c**)

Figure 5. Intensity-time profiles of SO_2^{+} ($m/z = 64$) in dependence of different pre-treatment methods. Raw wheat straw sample (**a**), torrefied sample (**b**), and (i) torrefied, then (ii) water-leached sample (**c**). The intensity-time profiles exemplify the effect of the applied pre-treatments. The torrefied and subsequently water-leached sample shows almost no more char gasification/ash reaction (**c**).

At the very beginning, a short volatile peak can be observed, which represents the pyrolysis peak, while in the second step, a significantly broader peak occurs, and this signal may explain the release of matter which is stronger chemically bound. Thus, the signal denotes the occurrence of the char gasification and ash reactions, which appear typically after the devolatilization process. The pyrolysis peak is characteristically denoted by a fast reaction kinetic, whereas the char gasification and the ash reaction is denoted by a slow kinetic rate.

The influence of both torrefaction and water-leaching can be clearly seen in the intensity-time profiles. Every sample shows a short peak at the very beginning (reddish area), which denotes a typical pyrolysis reaction. Although the raw material shows an obvious secondary release reaction in form of a broad ash/char reaction peak (greenish area), the torrefied and the torrefied/water-leached samples show only a range denoted by small intensity, which may be interpreted as ash/char reaction. Conversely, this means that sulfur compounds (most likely inorganic sulfates) can be successfully washed out by water-leaching. In addition, torrefaction showed a notable decreasing effect on the release behavior of SO_2. As mentioned by Knudsen et al. [37], it was observed that S is typically released in a mild temperature range (torrefaction temperature), as cysteine and methionine

start already decomposing at around 170–190 °C. Both cysteine and methionine are the main S-containing precursors for plant proteins [24].

In Figure 6, the normalized results of different peak areas are shown (both devolatilization and ash/char reaction).

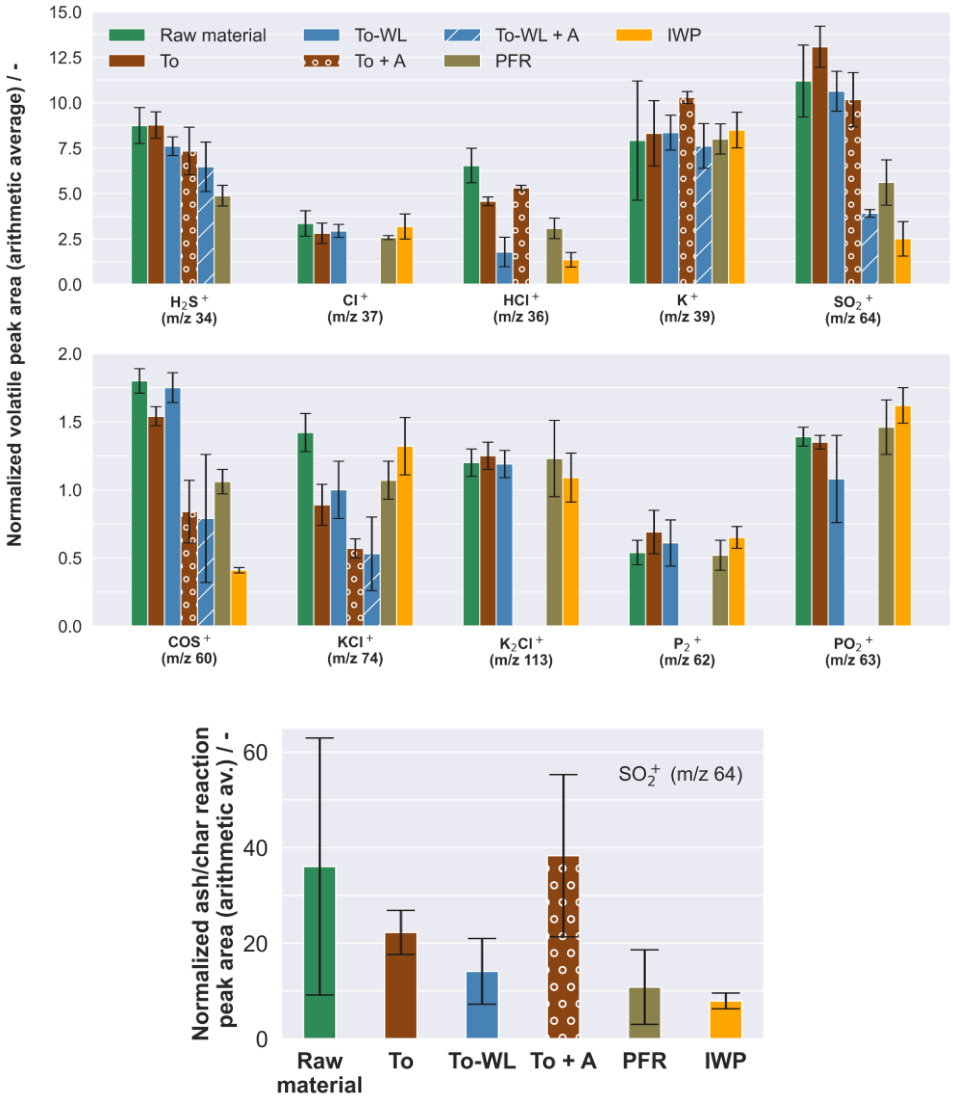

Figure 6. Averaged, normalized peak areas of species released during pyrolysis/devolatilization phase (**top**) and char gasification or ash reactions (**bottom**). For To-WL + A, no char gasification/ash reaction was observed.

Three measurements were performed per sample. Thus, large error bars typically illustrate the relatively high inhomogeneity of the herbaceous feedstocks in general. Nevertheless, certain trends can be observed. The release of hydrochloric acid (m/z = 36) is successfully decreased when the sample was (i) torrefied and then (ii) water-leached. Even torrefaction shows a decrease in the release of HCl. Keipi et al. [38] presented in their study how the concentration of chlorine dropped during torrefaction, since chlorine in biomass fuels may theoretically be reactive at torrefaction temperatures. As expected, the released amount of potassium chloride (m/z = 74) originating from the torrefied/water-leached sample is lower in contrast to the raw material. Interestingly, both woody feedstocks have shown, in general, a low content of released sulfur species (COS, SO_2, and H_2S) during gasification-like conditions, although the amount of sulfur in the ash seems to be approximately the same, such as in the herbaceous feedstock. The amount of released HCl is about

the same as for the torrefied/water-leached material, which represents an appropriate result at first appearance.

During the ash/char reaction, only the release of sulfur dioxide (m/z = 64) was observed, which originates from the decomposition and reaction of sulphates contained in the ash. Due to a short residence time in the flow-channel reactor, it is not reduced to H_2S in the gas phase despite the relatively low oxygen partial pressure and high water concentration. This, in turn, indicates that the hydrogen sulfide released during the devolatilization phase should mainly originate from sulfidic, primarily organically bound sulfur. Again, the wide dispersion of the error bar indicates a relatively high inhomogeneity of the raw material, meaning that the sulfur content varies from sample to sample. Both torrefaction and torrefaction/water-leaching decrease the amount of sulfur dioxide tendentially. Taking the ultimate analysis into account (Table 2), the industrial pine pellets have expectedly shown the lowest amount of released sulfur dioxide during ash/char reaction. When the straw sample is torrefied and then water-leached, almost the same amount of SO_2 is released as from IWP during the char gasification or ash reaction.

In addition to the torrefied and water-leached samples, Figure 6 exhibits the semi-quantitative analysis of the $CaCO_3$-blended samples (torrefied and torrefied/water-leached feedstock including 2 wt% $CaCO_3$, fuel-to-additive ratio). Interestingly, a slight decrease in the release can be observed for the sulfur-containing compounds H_2S, SO_2, and COS. In addition, a slight decrease in the release of KCl can be observed in comparison with the samples without additive (To and To-WL). Despite relatively inhomogeneous fuels, a slight trend can be seen here and the Ca-additive shows a noticeable effect on the release behavior of certain species. Figure 7 highlights the effect of Ca or the ratio of Ca to K in the sample on the amount of KCl, HCl or sulfur-containing species released during pyrolysis/devolatilization phase.

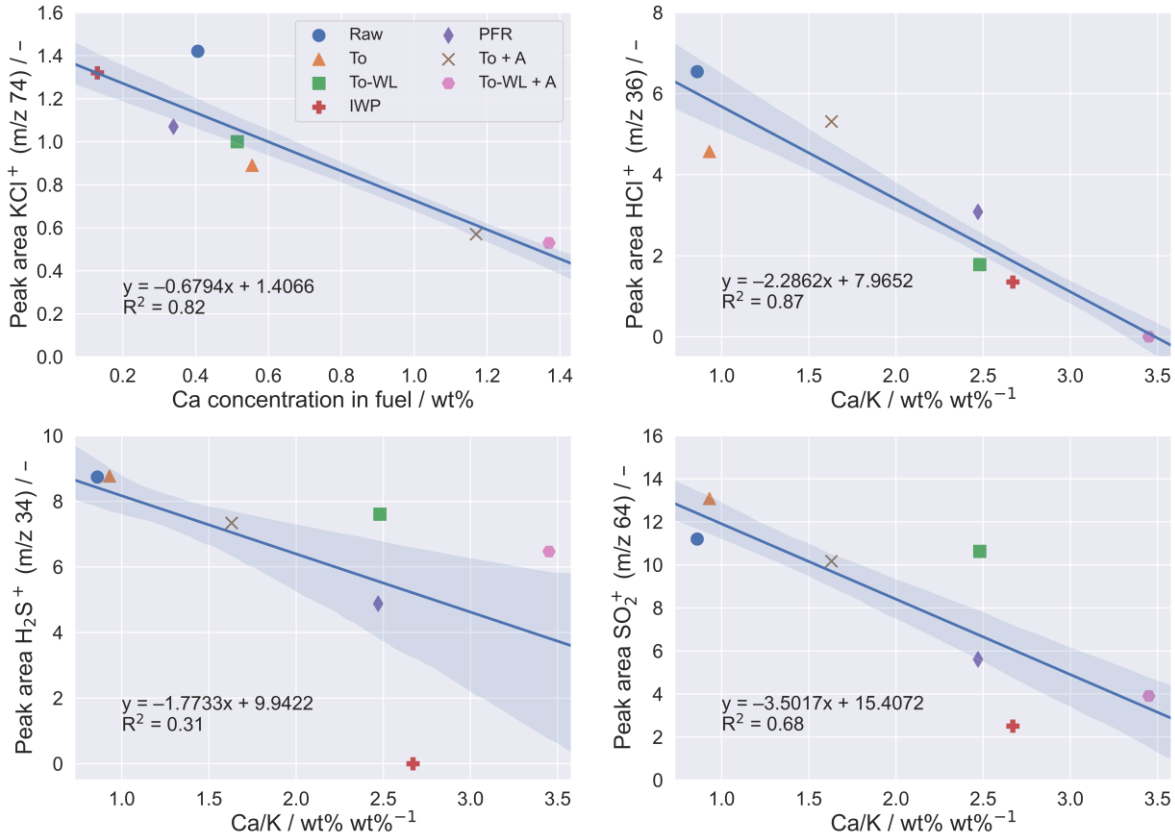

Figure 7. Correlation between the normalized volatile peak area (Figure 6) of KCl, HCl or sulfur-containing species and the concentration of Ca in the (pre-treated) fuel samples (**top-left**) or the weight ratio of Ca to K. The confidence interval is set at 68%.

It should be noted that the amount released should be considered as a semi-quantitative result. An increased amount of Ca in the fuel lowers the amount of KCl released. Although IWP, in contrast to To-WL + A, has a relatively low Ca content in the fuel, a corresponding higher amount of released KCl can be observed. Likewise, the higher the ratio of Ca to K, the lower the amount of HCl, H_2S and SO_2. Ca found in the sample is expected to form CaO instead of $CaCO_3$ as major ash component at a high temperature (950 °C). CaO may act as HCl sorbent according to

$$2HCl + CaO \rightarrow CaCl_2 + H_2O. \quad (5)$$

Similar observations were reported by Shemwell et al. [39], where HCl gas was treated using CaO, $CaCO_3$, and calcium formate with the result that high removal efficiencies were determined. In comparison with To-WL + A, To + A shows a stronger release of HCl. According to the ultimate analysis (Table 2), To + A shows a significantly higher K content, which conversely means that a higher KCl content must be present in the fuel sample. Possibly, CaO also reacts with KCl, according to Equation (6):

$$2KCl + CaO \rightarrow CaCl_2 + K_2O. \quad (6)$$

KCl is known to be the main source for HCl formation [35], which, in turn, might explain a decrease in HCl formation (besides the proposed reaction given in Equation (5)).

A likely explanation for the correlation between Ca and sulfur content might be given by the fact that Ca is an active suppressor for the release of the S species H_2S and SO_2 [35].

3.1.3. X-ray Powder Diffraction Analysis

Ash samples, prepared under gasification-like conditions, were investigated diffractometrically in order to understand the phase formation during gasification. In Figure 8, the recorded XRD spectra of the (pre-treated and/or $CaCO_3$-blended) feedstocks as well as IWP and PFR are presented.

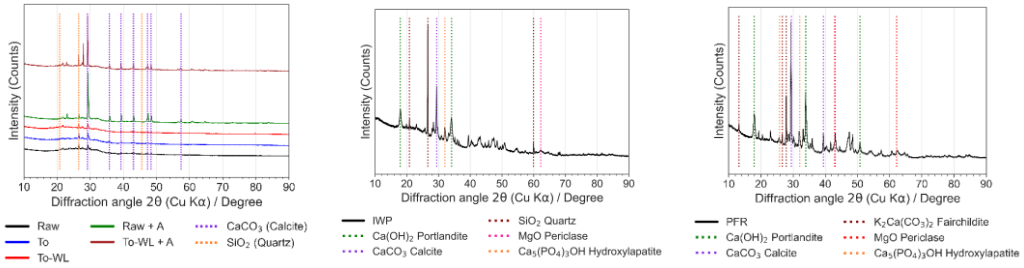

(**a**) (**b**) (**c**)

Figure 8. XRD spectra of the sample material (ashes): pre-treated and/or $CaCO_3$-blended wheat straw (**a**), industrial wood pellets (**b**), and pine forest residues (**c**).

As can be seen in Figure 8, the samples are predominantly amorphous. The low-temperature feedstock ash mostly consists of non-crystalline compounds, which are difficult to detect by means of XRD method [40]. This, in turn, means that a quantitative phase analysis by Rietveld method becomes difficult and inaccurate. A disadvantage of the applied XRD method is the morphology of the samples, since only crystalline compounds can be virtually evaluated. As the investigated ash samples show a relatively high amount of amorphous content, it can be assumed that they have the strongest impact on ash deposits formation, but they certainly cannot be detected by the XRD method [41,42].

However, the major phases, such as $CaCO_3$ or SiO_2, in the form of quartz could be evaluated. SiO_2 has been often determined in ashes produced from agricultural residues [43–45]. Both $CaCO_3$-blended feedstock ashes (raw and torrefied/water-leached) show the highest peak intensities concerning calcite. Even the samples, which have not

been blended, show small amounts of $CaCO_3$. No potassium chloride is detected in the samples, which might be explained by the fact that the chlorine content in the investigated samples is generally quite low. The chlorine content determined in all fuels was slightly above the measurement limit (note the ultimate analysis in Table 2), which, in turn, means that the major content must have been already washed out. Maybe the wheat straw feedstock has been stored on the field for longer time. Mason et al. [46] investigated the potassium content in the solid phase of different biomass materials, among others wheat straw. They found, in relation to the K content, that KCl when present, it is not necessarily the dominant species in the solid phase [46].

Both IWP and PFR have shown hydroxylapatite or portlandite. $Ca(OH)_2$ is typically formed when CaO reacts with water, and CaO, in turn, is formed when $CaCO_3$ decomposes at elevated temperature. P is primarily found in form of hydroxylapatite $Ca_5(PO_4)_3(OH)$ or calcium whitlockite (β-$Ca_3(PO_4)_2$) in the ashes from woody biomass [47]. Ca phosphates, such as hydroxylapatite or whitlockite, are more stable than the K–Ca phosphates and will therefore preferably be the final product [48].

The crystalline phase formation strongly depends on the ashing temperature. With increasing temperature some phases will form (e.g., silicates or aluminosilicates), but other phases will decompose, such as chlorides and carbonates [49]. Likewise, the heating rate might have a significant impact on the thermal characteristics of ash samples. Yang et al. [50] found that different heating rates showed a significant effect on fusion characteristics.

3.1.4. Ash Fusion Testing

The evaluation of the ash melting behavior investigated by hot stage microscopy (HSM) was carried out on the basis of Pang et al. [36] in relation to the initial height h_0 of the cylindrical ash sample and its corresponding change of height profile h_x during a stepwise heating process (coefficient h_x/h_0). The coefficient h_x/h_0, which is indirectly correlated with phase formations or transitions, is determined by shrinkage of the pellets. In Figure 9, the determined coefficients of the (pre-treated) samples are plotted in dependence of temperature. Results, which have been generated by HSM, are supposed to be a valuable indication of the ash melting behavior, especially relative behavior. Nevertheless, they are not supposed to be considered as absolute values because of the inhomogeneity of biomass-derived fuels (the ash melting behavior of different samples might show different characteristics) [51]. According to the determined height profile coefficient h_x/h_0, snapshots of the samples were taken for every temperature degree step (Figure 10).

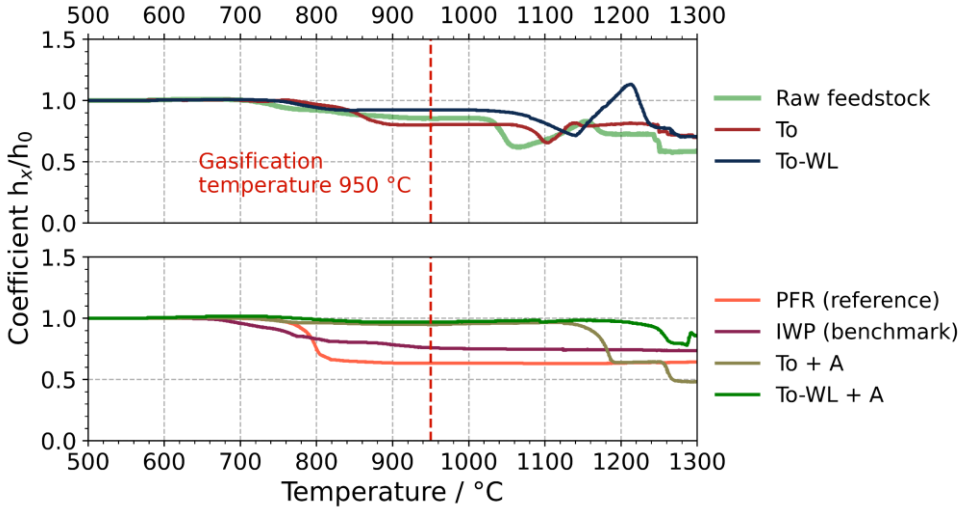

Figure 9. Height profile of ashes investigated by HSM in dependence of increasing temperature. The dashed red line denotes the defined gasification temperature of 950 °C.

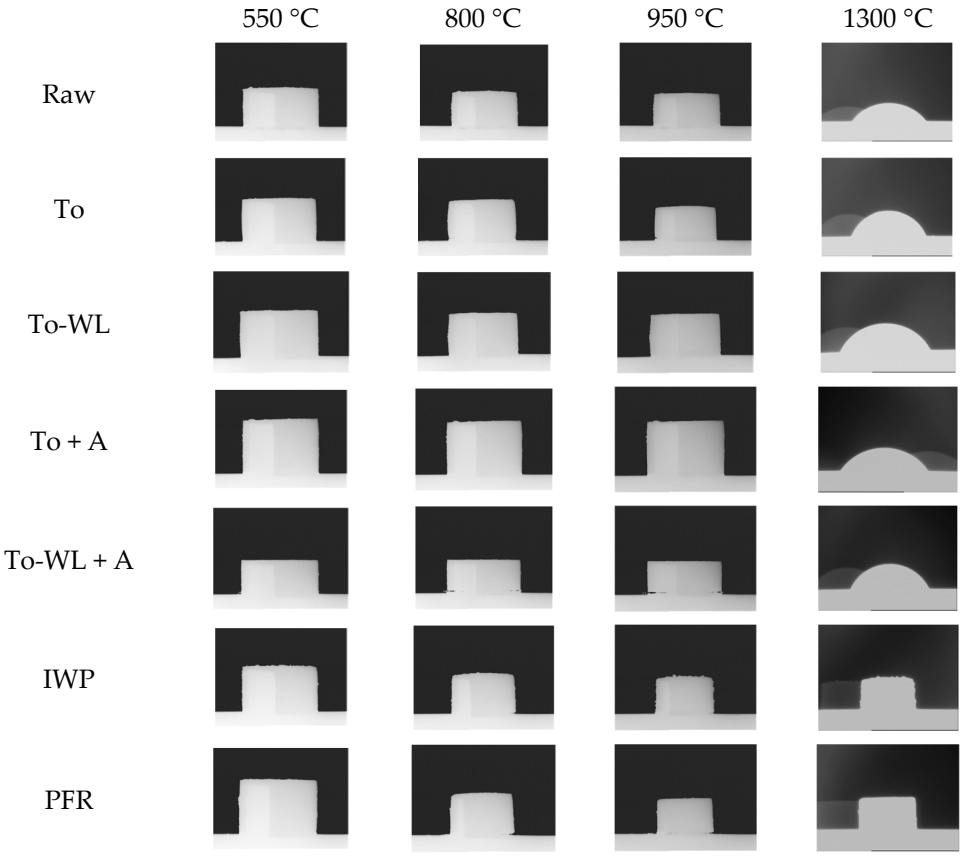

Figure 10. Snapshots recorded during ash fusion test. The change of the geometry of the pellets indicates first reactions or melting.

Raw straw ash starts slightly shrinking at 720 °C. However, no influence on agglomeration is expected in that case. The steep decrease in coefficient at 1020 °C indicates the start of melting while increases thereafter are likely caused by gas formation. In comparison, both IWP and PFR showed in a temperature range between 700 and 800 °C a noticeable, initial deformation in form of a pellet shrinkage, however, the size of the pellets remained stable until the end of the measurement (T_{end} = 1300 °C). For the pre-treated samples, it was observed that the slight initial deformation is shifted to approximately 750 °C and the severe deformation to 1050 °C. Moreover, a decrease in size was observed in a temperature range of 800 °C to 950 °C for the torrefied sample, where the ash behavior may become more problematic.

The most promising results were achieved by the $CaCO_3$-blended feedstocks. Both torrefied as well as torrefied/water-leached samples showed a relative stable geometrical profile up to higher temperature of 1120 °C and 1240 °C, respectively.

Therefore, they seem to be the most auspicious candidates. In reverse, this proves that the melting point is likewise increased. Nevertheless, the stability of the woody ash pellets seems to be highest at 1300 °C.

3.2. Thermodynamic Modelling

3.2.1. Release and Condensation of Volatile Inorganic Species

The gas phase fugacity for the most volatile inorganic components was calculated and is presented in Figure 11. The diagrams essentially display the same results as the experimental ones obtained in Figure 6, exhibiting a trend as a function of pre-treatment. In terms of the model calculations, the equilibrium is achieved in contrast to the experimental investigations, where usually no equilibrium is reached due to kinetic limitations.

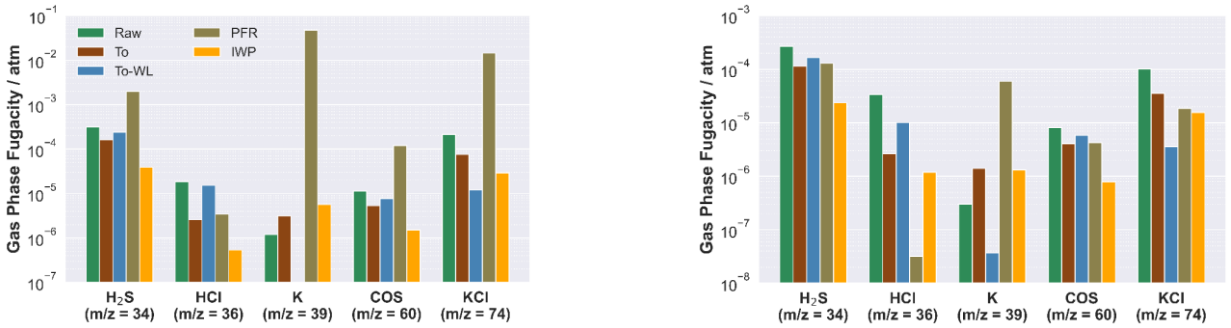

(**a**) (**b**)

Figure 11. Calculated gas phase fugacity of volatile species at isothermal conditions (950 °C) for pyrolysis-like conditions with no steam/oxygen added (**a**) and gasification-like conditions with steam/oxygen added (**b**).

For this reason, the thermodynamic model calculation, in contrast to the experimental approach, indicates different release behavior of volatile species (in terms of release intensity), which makes a direct comparison difficult.

In addition to the prediction of the release of volatile species into the gas phase, calculations on condensation of inorganic compounds (alkali chlorides, carbonates, and slag-mixtures) under gasification-like conditions, starting from 950 °C were performed. In Figure 12a, it can be observed that the condensation temperature of alkali chlorides released during gasification of pre-treated wheat straw varieties (both torrefied and torrefied/water-leached samples) are shifted towards lower temperatures. The amount of formed salts also decreased, when the wheat straw was treated. Torrefaction is known to decrease the amount of chlorine in feedstocks [38], thus, a lower content of chlorine provides a lower content of alkali chloride in turn. These observations are in a good agreement with the results obtained by chemical characterization (note the Cl content in Table 2). The condensation temperature of the alkali chlorides is found to be always lower than their corresponding melting points, which means that the salts should not be too sticky.

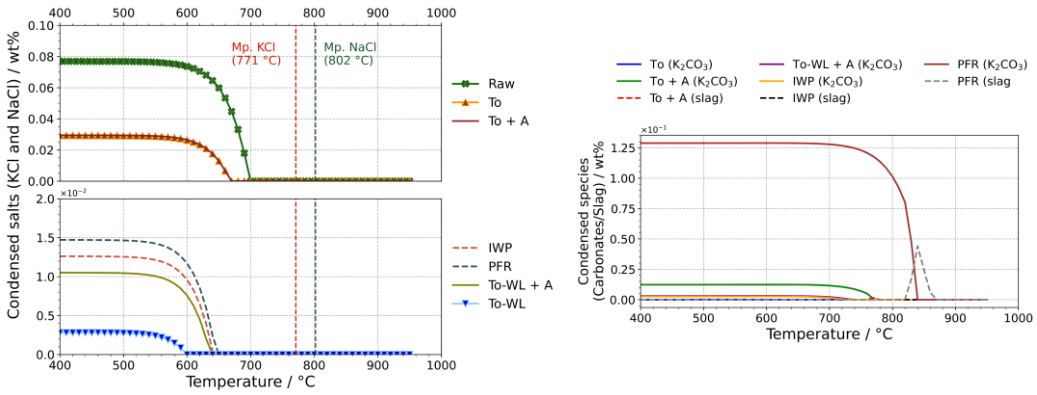

(**a**) (**b**)

Figure 12. Condensation of salts (mostly potassium chloride) (**a**) and carbonates, as well as slag-mixtures, mainly consisting of carbonates/sulfides (**b**), calculated under gasification-like conditions. The red and green dashed lines denote the corresponding melting temperatures of KCl and NaCl. The cooling temperature is 950 °C.

Moreover, the amount of formed salts of the torrefied/water-leached feedstocks seems to be decreased successfully when comparing with the raw feedstock. Blending the pre-treated samples with 2 wt% $CaCO_3$ does not seem to generally affect the quantitative

formation of both KCl and NaCl. Finally, the calculated amount of condensed salts for pine forest residues and industrial wood pellets is significantly lower than for wheat straw. In contrast, the formation of condensed carbonates (K_2CO_3 mainly) seems to be significantly higher than in (pre-treated) wheat straw, while IWP shows only small amounts of condensed carbonates. Additionally, considering the pine forest residues, a small amount of slag is condensing at around 840 °C. According to the predicted thermodynamic activities, mainly potassium sulfide was found in the slag. Interestingly, according to the shapes of both condensation curves, a typical phase formation can be observed, which means that potassium sulfide decomposed and potassium carbonate formed instead. Potassium sulfide becomes unstable beyond, as well as below its melting point, which explains the phase transition. This phenomenon was also observed in case of torrefied and $CaCO_3$-blended wheat straw samples. Both torrefied and torrefied/water-leached samples show small amounts of condensed carbonates. The thermodynamic equilibrium calculations did not exhibit any condensed carbonates for torrefied or torrefied/water-leached fuels without $CaCO_3$ additive.

In addition to the alkali salts, carbonates and sulfides, the condensation of liquid potassium cyanide was found for pine forest residues (only under pyrolysis conditions). Obviously, there should be a thermodynamic equilibrium in the temperature range between 700 °C and 820 °C, which favors the formation of KCN. Hansson et al. [52] reported that nitrogen-containing species, such as hydrogen cyanide, ammonia, and isocyanic acid, were identified while biomass-based feedstocks (amongst others bark pellets) have been pyrolyzed in a fluidized bed reactor at temperatures between 700 °C and 1000 °C.

3.2.2. Ash Behavior

Thermodynamic equilibrium calculations (performed by FactSage^{TM}) were used in order to predict inorganic phase formations of the (treated) material samples.

Based on the knowledge of the SiO_2-CaO-K_2O system, the fusibility tendencies can be predicted (Figure 13)—the main elements Ca, K, and Si, are responsible for agglomeration process [53]. The ash of the raw fuel is located in the liquid–solid two-phase-area and relatively close to the slag phase, while the ashes of IWP and PFR are located in the solid area. Woody biomass rather shows a noticeable lower K and Si content than WS (note the ultimate analysis in Table 2), which favors a high melting point of the ash. Torrefaction obviously does not seem to affect the ash melting behavior as already observed in the measurements performed by HSM. However, the other pre-treated samples show different behavior in terms of their phase states. According to the model calculation, torrefaction alone does not show the desired effect on the ash melting, while subsequent washing (To-WL) of the sample shows a positive effect on the ash melting. However, torrefaction of the sample and adding 2 wt% of $CaCO_3$ can suppress the ash melting, as the ash of the sample is located in the solid phase area.

The prediction of mineral phases was performed for both pyrolysis, as well as gasification conditions taking into account oxygen and steam. With regard to the formation of mineral phases, there was no major difference observed between pyrolysis and gasification reaction in general. This means that both processes seem to reveal the same reaction sequence. For the sake of clarity, only the calculated results of inorganic phase formations under gasification-like conditions are presented in the following. In the first step, all phases were numerically predicted in dependence of the temperature, starting from 400 °C and ending at 1300 °C. The main phases were summarized and sorted for a better overview (alkali chlorides, sulfides, carbonates and oxides/silicates). Figure 14 presents the calculated phase composition of the raw feedstock ash, in which the complete phases, as well as the grouped phases, are displayed.

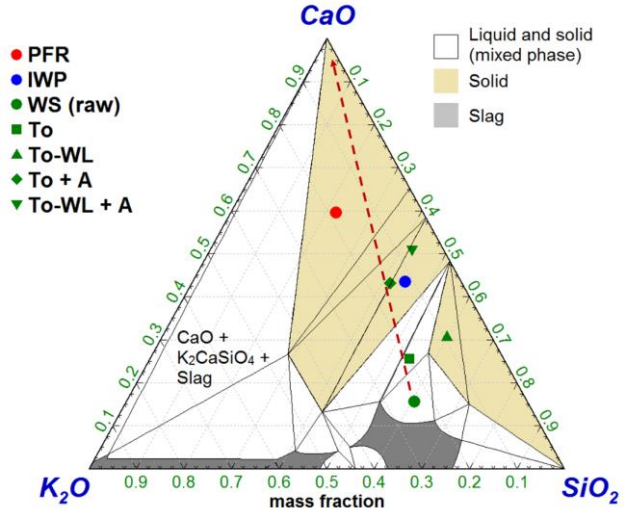

Figure 13. Calculated ternary phase diagram for the SiO_2-CaO-K_2O system using FactSage [32]. The phases were predicted for (pre-treated) wheat straw, as well as IWP (benchmark material) and PFR (chosen as alternative woody waste biomass). The calculation was performed under isothermal conditions at 950 °C.

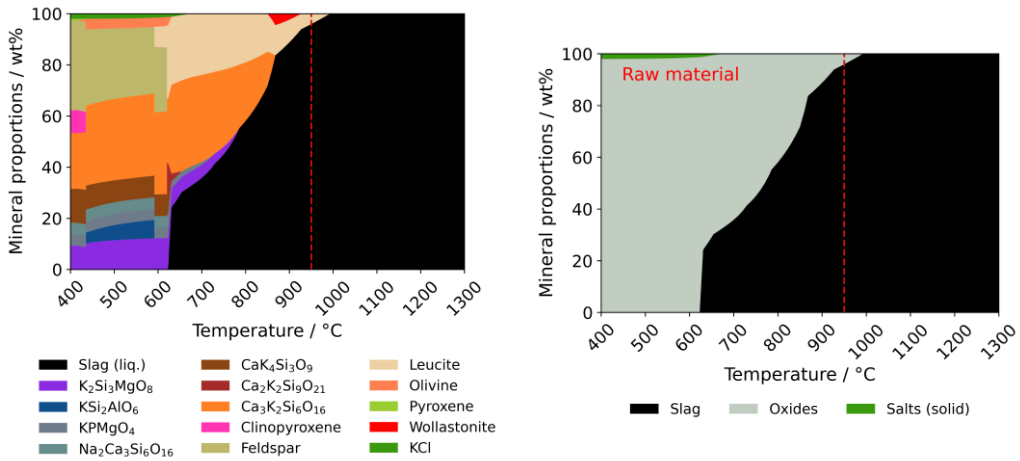

(**a**) (**b**)

Figure 14. Calculated mineral proportions of raw wheat straw ash under gasification-like conditions. (**a**) Overview phase map, where all predicted phases are mapped. (**b**) Summarized phases (mainly oxides and molten slag). The dashed red line denotes the gasification temperature of 950 °C.

The shape of the black area in Figure 14 is representing the amount of molten slag and can be considered as a pseudo-melting curve. The raw material shows at 950 °C (fixed gasification temperature in this study) over 90 wt% of molten slag. At 600 °C, on the other hand, mainly oxides in the solid state and small amounts of alkali metal salts were predicted. The amount of molten slag increases with increasing temperature. Figure 15 presents the predicted phase maps of each sample listed in Table 2.

IWP, which has been selected as benchmark material for this study, shows an amount of less than 40 wt% molten slag at 950 °C. The slag formation of the torrefied sample is shifted towards higher temperature in contrast to the raw material, approximately 100 °C. Even the content of alkali metal chlorides, as well as the amount of slag at gasification temperature is lower than in the raw feedstock. The observed effect is perceptible but not satisfying in the proper sense for the chemical looping gasification process, as reactors shall typically operate at temperatures above 900 °C. Torrefaction and subsequent water-leaching of the feedstock exhibit more promising results, and the quality of the benchmark

material can nearly be achieved. Obviously, the most reliable results are achieved when the torrefied or torrefied/water-leached material is blended with 2 wt% $CaCO_3$. In this case, a molten slag content of less than 20 wt% can be achieved. When blending the feedstock, a small amount of calcium-rich carbonates was found at lower temperatures. Since the content of calcium in the ash is significantly increased due to blending with the additive, the formation of carbonates is consequently favored. PFR shows a relatively high content of carbonates in contrast to the herbaceous feedstocks. The slag includes, but is not limited to, liquid carbonates, and this explains why the transition between carbonates and slag seems to proceed fluently in this case. No carbonates are found anymore at temperatures above 800 °C, as carbonates typically thermally decompose in this range.

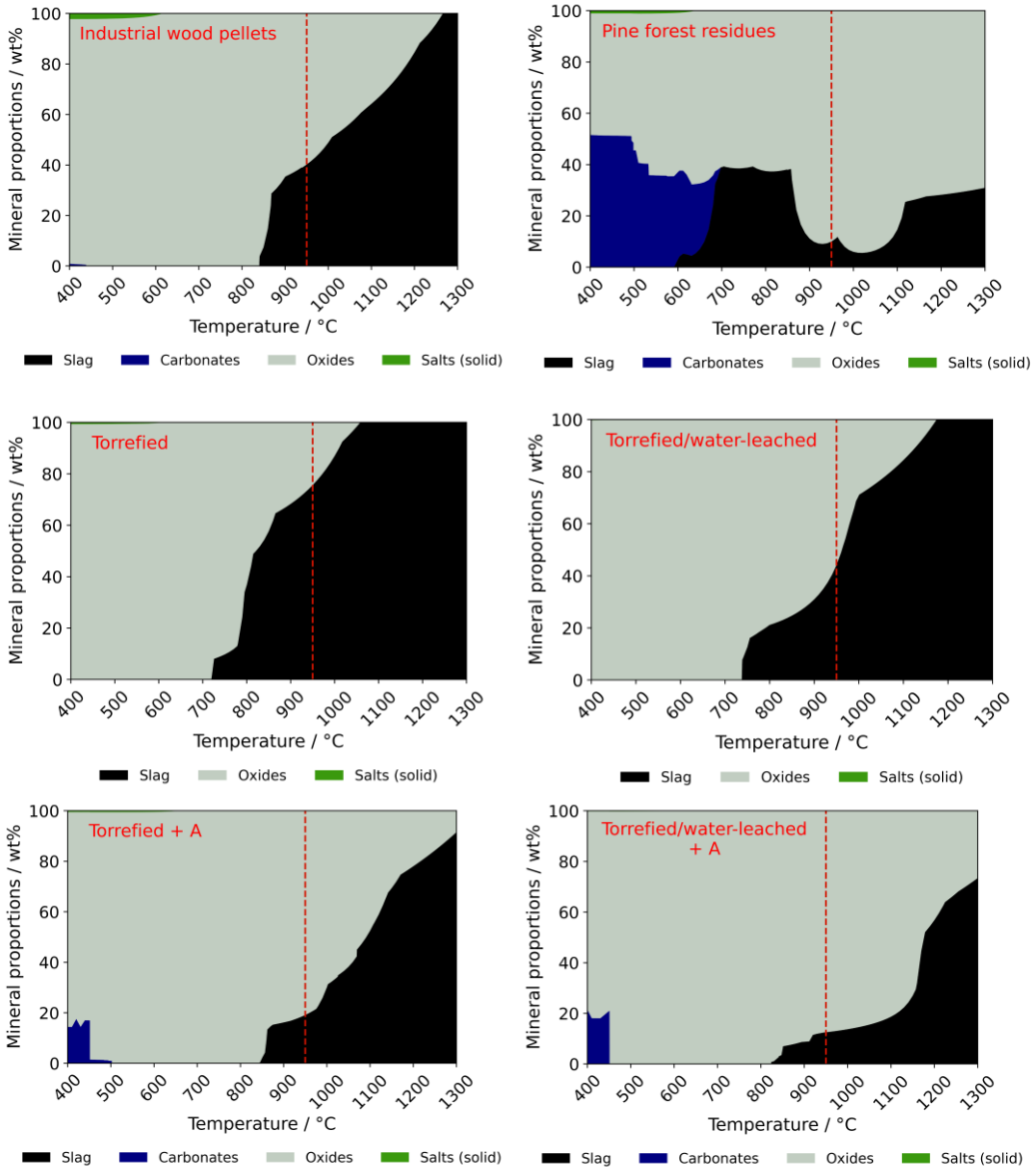

Figure 15. Calculated mineral proportions for industrial wood pellets, pine forest residues, and pre-treated or $CaCO_3$-blended wheat straw ash. The dashed line denotes the fixed gasification temperature (950 °C).

In Figure 16, a summarized comparison of the investigated (pre-treated) feedstocks is presented. The information given in the bar chart was taken from the calculated phase maps in Figure 15.

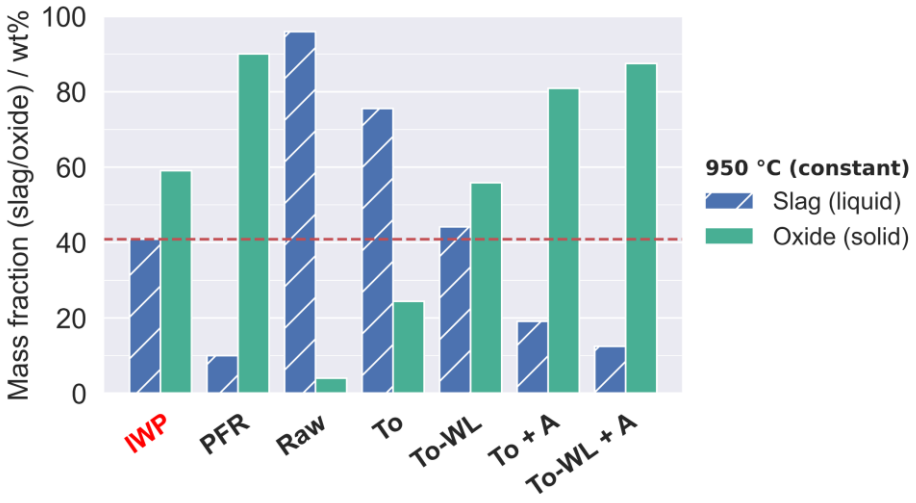

Figure 16. Comparison of the ash fusibility of the investigated samples (according to the calculated phase maps). The dashed red line denotes the amount of molten slag or solid oxides of the benchmark material IWP.

The formed amount of slag/oxides was calculated at gasification-like conditions (950 °C). The higher the slag part, the lower the amount of solid oxides and thus, the stickier the sample is. With about 10 wt%, PFR shows a relatively low amount of molten slag in comparison to the other samples.

3.2.3. Interaction and Poisoning of Oxygen Carrier Materials

Three different oxygen carrier materials were selected (LD Slag, Sibelco and Ilmenite), and interactions between the oxygen carriers and the fuel constituents were investigated in terms of the gas and condensed phase. The chemical composition of the oxygen carrier materials is listed in Table 3.

Table 3. Chemical composition of selected oxygen carriers (in wt%). Ilmenite contains additionally 5.5 wt% of inert materials, which have not been taken into account for thermodynamic calculations. Both Sibelco and Ilmenite were calcined.

Oxygen Carrier	MnO_2	Fe_2O_3	SiO_2	Al_2O_3	CaO	Fe_2TiO_5	TiO_2
LD Slag	5.42	26.85	14.08	1.29	52.36	-	-
Sibelco	72.99	9.05	7.31	7.97	2.67	-	-
Ilmenite	-	11.2	-	-	-	54.7	28.6

According to the thermodynamic flow chart (Figure 2), calculations under gasification conditions were performed, considering the following ratios: Oxygen carrier/fuel = 40/1, steam/fuel = 0.6 g/g, and air–fuel ratio λ = 0.3. The gasification temperature remains at 950 °C. The partial pressure was calculated for the most notable species and can be seen in Figure 17. Both Fe(II) hydroxide and aluminum hydroxide seem to keep constant in the gas phase and they are not affected by pre-treatment of samples. Since Sibelco shows the lowest iron and the highest aluminum content of the oxygen carriers, the partial pressure reflects the relative ratio. Interestingly, the partial pressure of orthosilicic acid is significantly lower in case of LD Slag than in case of Sibelco or Ilmenite. It is known that calcium binds silicon primarily as calcium silicates [54], thus lowering the activity of silica. Since LD Slag is almost half comprised of calcium oxide, silica is completely bound as calcium silicates, which suppress, in turn, the formation of orthosilicic acid. Both Fe(II) chloride and Mn(II) chloride prove, that chlorine, which is contained in wheat straw fuel, reacts with iron/manganese to form chloride compounds (with exception of Ilmenite, which does not contain any manganese). The torrefied and subsequently water-leached

sample shows an obvious decrease in the formation of volatile salts in comparison with the untreated source material.

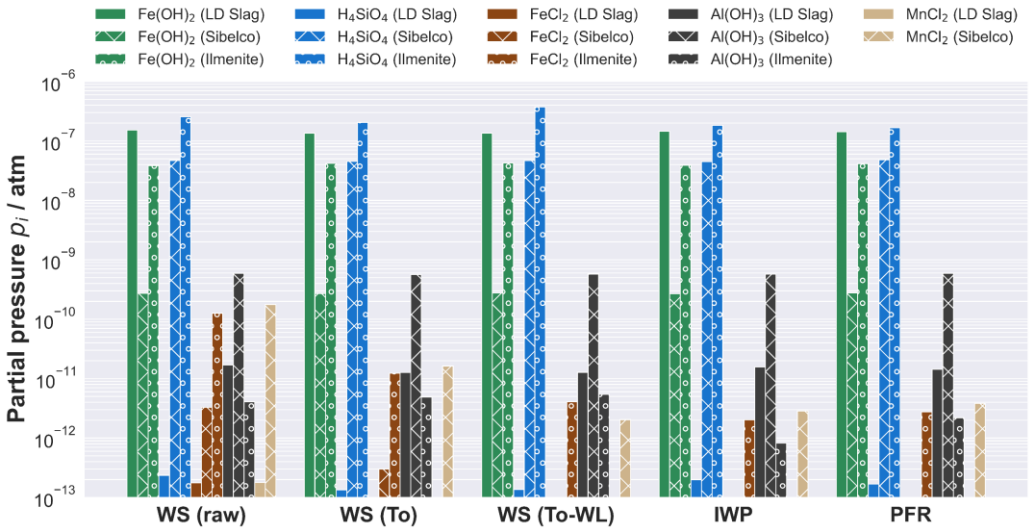

Figure 17. Predicted partial pressure of oxygen carrier constituents in contact with (pre-treated) wheat straw samples, as well as IWP and PFR under gasification-like, isothermal conditions (950 °C). The most important species, mainly in the range of $p_i > 10^{-12}$ atm are presented in dependence of the applied oxygen carrier (see Table 3).

Thermodynamic calculations with FactSage confirmed that mainly magnesium and potassium from the ash seem to interact with mineral phases from oxygen carriers to form intermediates and mixtures. For example, the ash of the raw as well as the torrefied material showed in combination with the titanium-rich oxygen carrier Ilmenite the formation of potassium titanate or even partially small amounts of sodium titanate ($K_2Ti_6O_{13}$, respectively, $Na_2Ti_6O_{13}$), which pictures a typical process of poisoning of the oxygen carrier in this case. When the samples were torrefied and washed before, no interactions between K and titania were observed anymore. The fact that water-leached samples show only small amounts of potassium, may explain the suppression of potassium titanate formation. According to the equilibrium calculations, both LD Slag and Sibelco did not show any interaction with the feedstock ash.

4. Discussion

Several investigation methods have been applied and combined to clarify the effect of pre-treatment methods and/or Ca-blending on inorganic constituents in wheat straw and their behavior and impact in chemical looping gasification. As already expected, the torrefied material showed a slightly higher content of ash in contrast to the raw material, while the torrefied/water-leached sample showed a lower content. The amount of ash of the Ca-blended feedstocks is also significantly higher. These results are consistent with the outcomes of the chemical characterization, as the ash only represents the non-combustible inorganic compounds. The woody fuels, both IWP and PFR, showed a relatively low ash content, as expected, due to their low amount of inorganic compounds. A lower ash content is conversely affiliated with a lower risk in terms of reactor operation. In the following sections, the most critical ash-related issues in CLG will be discussed and both experimental and calculated data as well are compared. In relation to the obtained results, conclusions are drawn about fouling and slagging, agglomeration, high-temperature corrosion, and poisoning of oxygen carriers.

4.1. Fouling and Slagging

The phenomenon of deposit formation on heat transfer surfaces (e.g., superheater tubes and boiler walls) is described by fouling and slagging, which is considered to cause two major problems associated with biomass fuel utilization [55]. The mineral deposits found on heat transfer surfaces are often comprised of alkali compounds [55]. Release experiments and thermodynamic equilibrium calculations in this study showed that mainly alkali salts and carbonates are released under typical CLG conditions, which condense in colder parts of the plant. In turn, this means that the higher the amount of volatile alkali compounds in biomass, the higher the potential risk of issues caused by condensation. Both torrefied and most notably water-leached wheat straw samples achieved the highest shift in predicted condensation temperature of alkali salts in comparison with the raw feedstock, thus showing almost the same condensation behavior as IWP. Therefore, these results seem to be promising, as the condensation temperatures of KCl (and partially NaCl) are much lower than their melting points and, thus, the deposits should not be too sticky for industrial scale application.

4.2. Bed Agglomeration

The phenomenon of bed agglomeration is a further obstacle, which describes the interaction between the molten or sticky ash compounds and the bed material. In consequence, the agglomeration causes a defluidization and, finally, a shutdown of the reactor unit. Both ash fusion tests (performed by HSM) and thermodynamic modelling have confirmed that torrefaction of the samples slightly decreased the melt fraction at 950 °C and the ash melting point was lightly increased. However, the effect is far from being sufficient for industrial application, as the amount of molten slag is still too high. In contrast to the torrefied samples, the torrefied/water-leached ones are more promising, as the effect of increasing the melting point is obviously more pronounced. It should also be noticed that the absolute amount of ash is generally decreased by pre-treatment versions of the feedstock, which can positively reduce the risk of bed agglomeration due to higher ratio of bed material to (molten) ash. In comparison with IWP as benchmark, the ashes of torrefied/water-leached fuels showed nearly an appropriate melting behavior. Both samples (To and To-WL), which have been blended with 2 wt% $CaCO_3$ (carbonate-to-feedstock-ratio) are the most promising candidates, and the results obtained by HSM and thermodynamic modelling are consistent with each other. Considering a gasification temperature of 950 °C, melting should not cause any problems in this case. The calculated amount of molten slag for both samples was even lower than for the benchmark material. Although IWP indicated a slag/oxide ratio of 40/60, the torrefied sample (incl. additive) showed and ratio of 20/80 and the torrefied/water-leached sample (incl. additive) a ratio of nearly 10/90. These results are in a good accordance with the experimental ash fusion tests. At this point, it has to be mentioned, that the major impact on melting temperatures of the sample ashes is influenced by the presence and concentration of alkali metals and the possibility of low-melting eutectics formation [49].

Another feasible option would be to apply To-WL feedstock without any (Ca-based) additives, however, in view of the predicted results, it would be more favorable then decreasing the gasification temperature from 950 °C to 900 °C or lower. No ash-related problems should occur then, and the expected phase formations should be similar to IWP.

4.3. High-Temperature Corrosion

Biomass contains in general a high amount of chlorine, which has a negative effect on the metal behavior, as it is directly correlated to chlorine induced corrosion [56]. The release experiments have highlighted that the method of torrefaction/water-leaching significantly influences the amount chlorides released during ash reactions. Since To-WL samples showed a lower ash content than the raw material, the amount of reactive inorganic species remained in the feedstock is decreased. In case of the benchmark material IWP, the amount of HCl released was almost similar. However, the effect of torrefaction or torrefaction/water-

leaching on the release behavior can also be clearly displayed in that case. Both torrefaction and water-leaching combined decrease the content of problematic inorganic species in the ash. Thus, torrefaction is not sufficient for application in an industrial scale, while the combination with water-leaching seems to be promising for removing problematic species. In addition to the influence on the ash melting behavior, the $CaCO_3$-additive has shown a slight effect on the release behavior of inorganic compounds, mainly sulfur-containing species. From a thermodynamic point of view, CaO or $CaCO_3$ can react with sulfur oxides in the temperature range 800–950 °C [57–60]. It is known that calcium reacts with SO_2 to form calcium sulfate and thus reduces SO_2 emissions [61]. In addition, a slight decrease in released amount of KCl was observed. It has been suggested elsewhere that Ca, S, and P may contribute to the capture and deposition of gaseous alkali chlorides (KCl or NaCl) [62–64]. A resulting formation of sulfates from the $CaCO_3$ additive and various sulfur species (H_2S, SO_2, COS) originating from the fuels could possibly also lead to a reduced release of KCl. The formation of alkali chlorides through different sulfation reactions can be decreased by sulfur-based additives [65–67].

Results obtained by thermodynamic modelling are in general consistent with the experimental ones, as obviously observable deviations occur in some cases. It should be mentioned that the calculations are only representing a thermodynamic model (which is based on Gibbs free energy minimization) and do not always correspond to kinetically controlled, real-experimental conditions. Therefore, inconsistency can be observed in that case.

4.4. Oxygen Carrier Poisoning

The backbone of any CLG application is the oxygen carrier material. In addition to the above-mentioned problems, oxygen carriers suffer reactions with ash-derived particles and the gas phase as well. For example, it is known that sulfur poisons the oxygen carrier activity [68]. Thermodynamic equilibrium calculations have indicated that chlorine (derived from the gas phase) might interact with iron and manganese in LD Slag, Sibelco and Ilmenite to form corresponding volatile chlorides. This effect can be counteracted by torrefying and/or water-leaching the samples, as chlorine can be successfully washed out of the feedstock. Thus, due to a lower amount of chlorine, the risk of poisoning is also reduced. Furthermore, according to predicted results, alkali and alkaline earth oxides can be incorporated in several solid phases of the oxygen carriers. In case of Ilmenite, alkali titanates should be formed. However, it should be mentioned here that torrefied/water-leached wheat straw has shown the most promising effect to reduce this risk.

5. Conclusions

Combination of various biomass pre-treatment technologies can be instrumental in boosting the bioeconomy as a whole. The main objective is to enable the fuel flexibility and to reduce logistical challenges and high transportation costs. Treatment of biomass aims at converting a feedstock into a fuel showing similar characteristics to that of original fossil fuels, which, in turn, becomes attractive for saving costs and lowering the impact on plant performance.

Different pre-treatment methods, based on water-leaching and torrefaction, as well as blending wheat straw with $CaCO_3$ were applied and their influence on the behavior of ash constituents was investigated in this study by different experimental methods and thermodynamic modelling. Results obtained by thermodynamic modelling are, in general, consistent with the experimental ones, as obviously deviations occur in some cases (e.g., when comparing the results obtained by experimental hot gas analysis, and calculated gas phase fugacity of volatile species). Note that the calculations are representing only a thermodynamic model and do not always correspond to kinetically controlled, real-experimental conditions. Therefore, inconsistency can be observed in that case.

The provided results shall contribute to tackling ash-related issues, such as agglomeration, fouling and slagging, poisoning of oxygen carriers, or high-temperature corrosion, which are representing typical problems during CLG process. According to the obtained

results, dry torrefaction can be considered as an effective pre-treatment method for removing chlorine. However, torrefaction is not effective enough for removing problematic species, such as alkalis. It increases the material density (the amount of ash is slightly increased), which means that it eliminates volatile organic compounds and water. Summarizing the above, it can be said that torrefaction can be considered as a de-chlorinating process, which can prevent the formation of related pollutants, as well as the accelerated corrosion in the thermochemical process. Torrefaction combined with water-leaching seems to be more promising in terms of removing problematic species, such as alkali chlorides or even partially sulfur compounds. Torrefaction/water-leaching has successfully decreased the amount of molten slag formed at a gasification temperature of 950 °C. The "quality" of the benchmark material IWP was almost reached. The most promising results regarding ash melting behavior were achieved when pre-treated (both To and To-WL) wheat straw was blended with 2 wt% $CaCO_3$. Samples including additives have shown that their ash melting point could be increased significantly (thermodynamic modelling and HSM measurements), while the release of chlorine and sulfur species is reduced (MBMS measurements), so that the utilization in a fluidized bed seems to be feasible. In summary, one can say that torrefaction alone is not effective enough for removing problematic species or increasing the ash melting point for the wheat straw under investigation. Basically, both experimental investigations and thermodynamic equilibrium calculations confirmed that combination of pre-treatment methods seem more promising. Therefore, this approach should be validated in future studies in pilot plants.

Author Contributions: The authors contributed as follows: Conceptualization, F.L. and M.M.; methodology, F.L. and M.M.; software, F.L.; validation, F.L.; formal analysis, F.L.; investigation, F.L.; resources, I.F., R.P.-V. and M.M.; data curation, F.L., R.P.-V. and M.M.; writing—original draft preparation, F.L.; writing—review and editing, F.L., M.M., R.P.-V. and I.F.; visualization, F.L.; supervision, M.M.; project administration, M.M.; funding acquisition, M.M. All authors have read and agreed to the published version of the manuscript.

Funding: This research was funded by the Horizon 2020 Framework program of the European Union, CLARA project, G.A. 817841.

Institutional Review Board Statement: Not applicable.

Informed Consent Statement: Not applicable.

Data Availability Statement: Not applicable.

Conflicts of Interest: The authors declare no conflict of interest. The funders had no role in the design of the study; in the collection, analyses, or interpretation of data; in the writing of the manuscript, or in the decision to publish the results.

References

1. United Nations. Paris Climate Agreement. 2015. Available online: https://unfccc.int/process-and-meetings/the-paris-agreement/the-paris-agreement (accessed on 29 March 2022).
2. Cherubini, F.; Peters, G.P.; Berntsen, T.; Strømman, A.H.; Hertwich, E. CO_2 emissions from biomass combustion for bioenergy: Atmospheric decay and contribution to global warming. *GCB Bioenergy* **2011**, *3*, 413–426. [CrossRef]
3. Mohamed, U.; Zhao, Y.; Huang, Y.; Cui, Y.; Shi, L.; Li, C.; Pourkashanian, M.; Wei, G.; Yi, Q.; Nimmo, W. Sustainability evaluation of biomass direct gasification using chemical looping technology for power generation with and w/o CO_2 capture. *Energy* **2020**, *205*, 117904. [CrossRef]
4. Ishida, M.; Zheng, D.; Akehata, T. Evaluation of a chemical-looping-combustion power-generation system by graphic exergy analysis. *Energy* **1987**, *12*, 147–154. [CrossRef]
5. Huang, Z.; He, F.; Feng, Y.; Zhao, K.; Zheng, A.; Chang, S.; Wei, G.; Zhao, Z.; Li, H. Biomass char direct chemical looping gasification using NiO-modified iron ore as an oxygen carrier. *Energy Fuels* **2014**, *28*, 183–191. [CrossRef]
6. Huang, Z.; He, F.; Zheng, A.; Zhao, K.; Chang, S.; Zhao, Z.; Li, H. Synthesis gas production from biomass gasification using steam coupling with natural hematite as oxygen carrier. *Energy* **2013**, *53*, 244–251. [CrossRef]
7. Ge, H.; Guo, W.; Shen, L.; Song, T.; Xiao, J. Biomass gasification using chemical looping in a 25 kWth reactor with natural hematite as oxygen carrier. *Chem. Eng. J.* **2016**, *286*, 174–183. [CrossRef]

8. Nguyen, N.M.; Alobaid, F.; Dieringer, P.; Epple, B. Biomass-Based Chemical Looping Gasification: Overview and Recent Developments. *Appl. Sci.* **2021**, *11*, 7069. [CrossRef]
9. CLARA. Chemical Looping Gasification for Sustainable Production of Biofuels. Available online: https://clara-h2020.eu/ (accessed on 29 March 2022).
10. Zeng, T.; Mlonka-Mędrala, A.; Lenz, V.; Nelles, M. Evaluation of bottom ash slagging risk during combustion of herbaceous and woody biomass fuels in a small-scale boiler by principal component analysis. *Biomass Convers. Biorefinery* **2021**, *11*, 1211–1229. [CrossRef]
11. Demirbaş, A. Demineralization of agricultural residues by water leaching. *Energy Sources* **2003**, *25*, 679–687. [CrossRef]
12. Boström, D.; Grimm, A.; Boman, C.; Björnbom, E.; Ohman, M. Influence of kaolin and calcite additives on ash transformations in small-scale combustion of oat. *Energy Fuels* **2009**, *23*, 5184–5190. [CrossRef]
13. Kassman, H.; Pettersson, J.; Steenari, B.-M.; Åmand, L.-E. Two strategies to reduce gaseous KCl and chlorine in deposits during biomass combustion—Injection of ammonium sulphate and co-combustion with peat. *Fuel Process. Technol.* **2013**, *105*, 170–180. [CrossRef]
14. Baxter, L.L.; Miles, T.R.; Miles, T.R., Jr.; Jenkins, B.M.; Milne, T.; Dayton, D.; Bryers, R.W.; Oden, L.L. The behavior of inorganic material in biomass-fired power boilers: Field and laboratory experiences. *Fuel Process. Technol.* **1998**, *54*, 47–78. [CrossRef]
15. Vassilev, S.V.; Baxter, D.; Vassileva, C.G. An overview of the behaviour of biomass during combustion: Part II. Ash fusion and ash formation mechanisms of biomass types. *Fuel* **2014**, *117*, 152–183. [CrossRef]
16. Wang, Y.; Wu, H.; Sárossy, Z.; Dong, C.; Glarborg, P. Release and transformation of chlorine and potassium during pyrolysis of KCl doped biomass. *Fuel* **2017**, *197*, 422–432. [CrossRef]
17. Zeng, T.; Weller, N.; Pollex, A.; Lenz, V. Blended biomass pellets as fuel for small scale combustion appliances: Influence on gaseous and total particulate matter emissions and applicability of fuel indices. *Fuel* **2016**, *184*, 689–700. [CrossRef]
18. Katsaros, G.; Sommersacher, P.; Retschitzegger, S.; Kienzl, N.; Tassou, S.A.; Pandey, D.S. Combustion of poultry litter and mixture of poultry litter with woodchips in a fixed bed lab-scale batch reactor. *Fuel* **2021**, *286*, 119310. [CrossRef]
19. Sommersacher, P.; Brunner, T.; Obernberger, I. Fuel indexes: A novel method for the evaluation of relevant combustion properties of new biomass fuels. *Energy Fuels* **2012**, *26*, 380–390. [CrossRef]
20. Qian, X.; Xue, J.; Yang, Y.; Lee, S.W. Thermal properties and combustion-related problems prediction of agricultural crop residues. *Energies* **2021**, *14*, 4619. [CrossRef]
21. Anukam, A.; Mamphweli, S.; Reddy, P.; Meyer, E.; Okoh, O. Pre-processing of sugarcane bagasse for gasification in a downdraft biomass gasifier system: A comprehensive review. *Renew. Sustain. Energy Rev.* **2016**, *66*, 775–801. [CrossRef]
22. Chiang, K.-Y.; Chien, K.-L.; Lu, C.-H. Characterization and comparison of biomass produced from various sources: Suggestions for selection of pretreatment technologies in biomass-to-energy. *Appl. Energy* **2012**, *100*, 164–171. [CrossRef]
23. Barskov, S.; Zappi, M.; Buchireddy, P.; Dufreche, S.; Guillory, J.; Gang, D.; Hernandez, R.; Bajpai, R.; Baudier, J.; Cooper, R.; et al. Torrefaction of biomass: A review of production methods for biocoal from cultured and waste lignocellulosic feedstocks. *Renew. Energy* **2019**, *142*, 624–642. [CrossRef]
24. Saleh, S.B.; Flensborg, J.P.; Shoulaifar, T.K.; Sárossy, Z.; Hansen, B.B.; Egsgaard, H.; DeMartini, N.; Jensen, P.A.; Glarborg, P.; Dam-Johansen, K. Release of chlorine and sulfur during biomass torrefaction and pyrolysis. *Energy Fuels* **2014**, *28*, 3738–3746. [CrossRef]
25. Yu, C.; Thy, P.; Wang, L.; Anderson, S.N.; VanderGheynst, J.S.; Upadhyaya, S.K.; Jenkins, B.M. Influence of leaching pretreatment on fuel properties of biomass. *Fuel Process. Technol.* **2014**, *128*, 43–53. [CrossRef]
26. Gong, S.H.; Im, H.S.; Um, M.; Lee, H.W.; Lee, J.W. Enhancement of waste biomass fuel properties by sequential leaching and wet torrefaction. *Fuel* **2019**, *239*, 693–700. [CrossRef]
27. Zhang, S.; Su, Y.; Xu, D.; Zhu, S.; Zhang, H.; Liu, X. Effects of torrefaction and organic-acid leaching pretreatment on the pyrolysis behavior of rice husk. *Energy* **2018**, *149*, 804–813. [CrossRef]
28. Chaloupková, V.; Ivanova, T.; Hutla, P.; Špunarová, M. Ash Melting Behavior of Rice Straw and Calcium Additives. *Agriculture* **2021**, *11*, 1282. [CrossRef]
29. Zheng, A.; Zhao, Z.; Chang, S.; Huang, Z.; Zhao, K.; Wei, G.; He, F.; Li, H. Comparison of the effect of wet and dry torrefaction on chemical structure and pyrolysis behavior of corncobs. *Bioresour. Technol.* **2015**, *176*, 15–22. [CrossRef]
30. Lynam, J.G.; Coronella, C.J.; Yan, W.; Reza, M.T.; Vasquez, V.R. Acetic acid and lithium chloride effects on hydrothermal carbonization of lignocellulosic biomass. *Bioresour. Technol.* **2011**, *102*, 6192–6199. [CrossRef]
31. Tu, R.; Jiang, E.; Yan, S.; Xu, X.; Rao, S. The pelletization and combustion properties of torrefied Camellia shell via dry and hydrothermal torrefaction: A comparative evaluation. *Bioresour. Technol.* **2018**, *264*, 78–89. [CrossRef]
32. Bale, C.W.; Bélisle, E.; Chartrand, P.; Decterov, S.A.; Eriksson, G.; Gheribi, A.E.; Hack, K.; Jung, I.-H.; Kang, Y.-B.; Melançon, J.; et al. Reprint of: FactSage thermochemical software and databases, 2010–2016. *Calphad* **2016**, *55*, 1–19. [CrossRef]
33. Yazhenskikh, E.; Jantzen, T.; Hack, K.; Müller, M. A new multipurpose thermodynamic database for oxide systems. *Расплавы* **2019**, *2*, 116–124. [CrossRef]
34. Bläsing, M.; Müller, M. Mass spectrometric investigations on the release of inorganic species during gasification and combustion of German hard coals. *Combust. Flame* **2010**, *157*, 1374–1381. [CrossRef]
35. Bläsing, M.; Zini, M.; Müller, M. Influence of feedstock on the release of potassium, sodium, chlorine, sulfur, and phosphorus species during gasification of wood and biomass shells. *Energy Fuels* **2013**, *27*, 1439–1445. [CrossRef]

36. Pang, C.H.; Hewakandamby, B.; Wu, T.; Lester, E. An automated ash fusion test for characterisation of the behaviour of ashes from biomass and coal at elevated temperatures. *Fuel* **2013**, *103*, 454–466. [CrossRef]
37. Knudsen, J.N.; Jensen, P.A.; Lin, W.; Frandsen, F.J.; Dam-Johansen, K. Sulfur transformations during thermal conversion of herbaceous biomass. *Energy Fuels* **2004**, *18*, 810–819. [CrossRef]
38. Keipi, T.; Tolvanen, H.; Kokko, L.; Raiko, R. The effect of torrefaction on the chlorine content and heating value of eight woody biomass samples. *Biomass Bioenergy* **2014**, *66*, 232–239. [CrossRef]
39. Shemwell, B.; Levendis, Y.A.; Simons, G.A. Laboratory study on the high-temperature capture of HCl gas by dry-injection of calcium-based sorbents. *Chemosphere* **2001**, *42*, 785–796. [CrossRef]
40. Vassilev, S.V.; Baxter, D.; Andersen, L.K.; Vassileva, C.G.; Morgan, T.J. An overview of the organic and inorganic phase composition of biomass. *Fuel* **2012**, *94*, 1–33. [CrossRef]
41. Tiainen, M.S.; Ryynänen, J.S.; Rantala, J.T.; Patrikainen, H.T.; Laitinen, R.S. Determination of Amorphous Material in Peat Ash by X-ray Diffraction. In *Impact of Mineral Impurities in Solid Fuel Combustion*, 1st ed.; Gupta, R.P., Wall, T.F., Baxter, L., Eds.; Springer: New York, NY, USA, 2002; pp. 217–224.
42. Ward, C.R. Mineral Characterization for Combustion. In *Impact of Mineral Impurities in Solid Fuel Combustion*, 1st ed.; Gupta, R.P., Wall, T.F., Baxter, L., Eds.; Springer: New York, NY, USA, 2002; pp. 23–32.
43. Steenari, B.-M.; Lundberg, A.; Pettersson, H.; Wilewska-Bien, M.; Andersson, D. Investigation of ash sintering during combustion of agricultural residues and the effect of additives. *Energy Fuels* **2009**, *23*, 5655–5662. [CrossRef]
44. Gilbe, C.; Ohman, M.; Lindström, E.; Boström, D.; Backman, R.; Samuelsson, R.; Burvall, J. Slagging characteristics during residential combustion of biomass pellets. *Energy Fuels* **2008**, *22*, 3536–3543. [CrossRef]
45. Steenari, B.-M.; Lindqvist, O. High-temperature reactions of straw ash and the anti-sintering additives kaolin and dolomite. *Biomass Bioenergy* **1998**, *14*, 67–76. [CrossRef]
46. Mason, P.E.; Darvell, L.I.; Jones, J.M.; Williams, A. Observations on the release of gas-phase potassium during the combustion of single particles of biomass. *Fuel* **2016**, *182*, 110–117. [CrossRef]
47. Bostrom, D.; Skoglund, N.; Grimm, A.; Boman, C.; Ohman, M.; Brostrom, M.; Backman, R. Ash transformation chemistry during combustion of biomass. *Energy Fuels* **2012**, *26*, 85–93. [CrossRef]
48. Hedayati, A.; Lindgren, R.; Skoglund, N.; Boman, C.; Kienzl, N.; Öhman, M. Ash Transformation during Single-Pellet Combustion of Agricultural Biomass with a Focus on Potassium and Phosphorus. *Energy Fuels* **2021**, *35*, 1449–1464. [CrossRef]
49. Mlonka-Mędrala, A.; Magdziarz, A.; Gajek, M.; Nowińska, K.; Nowak, W. Alkali metals association in biomass and their impact on ash melting behaviour. *Fuel* **2020**, *261*, 116421. [CrossRef]
50. Yang, J.; Feng, Z.; Ni, L.; Gao, Q.; He, Y.; Hou, Y.; Liu, Z. Thermal Characteristics of Ash from Bamboo and Masson Pine Blends: Influence of Mixing Ratio and Heating Rate. *ACS Omega* **2021**, *6*, 7008–7014. [CrossRef]
51. Toscano, G.; Corinaldesi, F. Ash fusibility characteristics of some biomass feedstocks and examination of the effects of inorganic additives. *J. Agric. Eng.* **2010**, *41*, 13–19. [CrossRef]
52. Hansson, K.-M.; Samuelsson, J.; Tullin, C.; Åmand, L.-E. Formation of HNCO, HCN, and NH3 from the pyrolysis of bark and nitrogen-containing model compounds. *Combust. Flame* **2004**, *137*, 265–277. [CrossRef]
53. Lindström, E.; Öhman, M.; Backman, R.; Boström, D. Influence of sand contamination on slag formation during combustion of wood derived fuels. *Energy Fuels* **2008**, *22*, 2216–2220. [CrossRef]
54. Risnes, H.; Fjellerup, J.; Henriksen, U.; Moilanen, A.; Norby, P.; Papadakis, K.; Posselt, D.; Sørensen, L.H. Calcium addition in straw gasification. *Fuel* **2003**, *82*, 641–651. [CrossRef]
55. Lachman, J.; Baláš, M.; Lisỳ, M.; Lisá, H.; Milčák, P.; Elbl, P. An overview of slagging and fouling indicators and their applicability to biomass fuels. *Fuel Process. Technol.* **2021**, *217*, 106804. [CrossRef]
56. Elger, R. High Temperature Corrosion in Biomass-Fired Energy Applications: Alloying Effects and Test Environment Comparisons. Ph.D. Thesis, KTH Royal Institute of Technology, Stockholm, Sweden, 2016.
57. Manovic, V.; Grubor, B.; Repić, B.; Mladenović, M.R.; Jovanović, M.P. Sulfur release during combustion of Serbian coals. *Fresenius Environ. Bull.* **2003**, *12*, 1348–1353.
58. Wieczorek-Ciurowa, K. Physico-chemistry of the limestone sulphation process. *J. Therm. Anal. Calorim.* **1998**, *54*, 85–91. [CrossRef]
59. Atilgan, İ. Investigation of the effect of particle size of limestone added to lignite on emission behavior in a fluidized bed combustion system. *Gazi Univ. J. Sci.* **2004**, *17*, 89–101.
60. Ilten, N.; Sungur, U. Removal of sulphur during combustion of coal by using lime. *Fresenius Environ. Bull.* **2009**, *18*, 2296–2301.
61. Pisupati, S.V.; Bhalla, S. Influence of Calcium Content of Biomass-Based Materials on Simultaneous NOx and SO_2 Reduction. *Environ. Sci. Technol.* **2008**, *42*, 2509–2514. [CrossRef]
62. Wang, L.; Skjevrak, G.; Hustad, J.E.; Skreiberg, Ø. Investigation of biomass ash sintering characteristics and the effect of additives. *Energy Fuels* **2014**, *28*, 208–218. [CrossRef]
63. Åmand, L.-E.; Leckner, B.; Eskilsson, D.; Tullin, C. Deposits on heat transfer tubes during co-combustion of biofuels and sewage sludge. *Fuel* **2006**, *85*, 1313–1322. [CrossRef]
64. Pettersson, A.; Zevenhoven, M.; Steenari, B.-M.; Åmand, L.-E. Application of chemical fractionation methods for characterisation of biofuels, waste derived fuels and CFB co-combustion fly ashes. *Fuel* **2008**, *87*, 3183–3193. [CrossRef]
65. Wang, L.; Hustad, J.E.; Skreiberg, Ø.; Skjevrak, G.; Grønli, M. A critical review on additives to reduce ash related operation problems in biomass combustion applications. *Energy Procedia* **2012**, *20*, 20–29. [CrossRef]

66. Shao, Y.; Wang, J.; Preto, F.; Zhu, J.; Xu, C. Ash deposition in biomass combustion or co-firing for power/heat generation. *Energies* **2012**, *5*, 5171–5189. [CrossRef]
67. Fournel, S.; Palacios, J.H.; Godbout, S.; Heitz, M. Effect of additives and fuel blending on emissions and ash-related problems from small-scale combustion of reed canary grass. *Agriculture* **2015**, *5*, 561–576. [CrossRef]
68. Wang, P.; Means, N.; Shekhawat, D.; Berry, D.; Massoudi, M. Chemical-looping combustion and gasification of coals and oxygen carrier development: A brief review. *Energies* **2015**, *8*, 10605–10635. [CrossRef]